HHS Public Access

Author manuscript

J Magn Reson Open. Author manuscript; available in PMC 2023 December 20.

Published in final edited form as:

J Magn Reson Open. 2023 December ; 16-17: . doi:10.1016/j.jmro.2023.100127.

CPMAS NMR platform for direct compositional analysis of mycobacterial cell-wall complexes and whole cells

Xinyu Liu[a], **Jasna Brčić**[a], **Gail H. Cassell**[b,c], **Lynette Cegelski**[a,*]

[a]Department of Chemistry, Stanford University, CA 94305, United States

[b]PAI Life Sciences Inc, Seattle WA 98102, United States

[c]Department of Global Health and Social Medicine, Harvard Medical School, Boston, MA 02115, United States

Abstract

Tuberculosis and non-tuberculosis mycobacterial infections are rising each year and often result in chronic incurable disease. Important antibiotics target cell-wall biosynthesis, yet some mycobacteria are alarmingly resistant or tolerant to currently available antibiotics. This resistance is often attributed to assumed differences in composition of the complex cell wall of different mycobacterial strains and species. However, due to the highly crosslinked and insoluble nature of mycobacterial cell walls, direct comparative determinations of cell-wall composition pose a challenge to analysis through conventional biochemical analyses. We introduce an approach to directly observe the chemical composition of mycobacterial cell walls using solid-state NMR spectroscopy. ^{13}C CPMAS spectra are provided of individual components (peptidoglycan, arabinogalactan, and mycolic acids) and of *in situ* cell-wall complexes. We assigned the spectroscopic contributions of each component in the cell-wall spectrum. We uncovered a higher arabinogalactan-to-peptidoglycan ratio in the cell wall of *M. abscessus*, an organism noted for its antibiotic resistance, relative to *M. smegmatis*. Furthermore, differentiating influences of different types of cell-wall targeting antibiotics were observed in spectra of antibiotic-treated whole cells. This platform will be of value in evaluating cell-wall composition and antibiotic activity among different mycobacteria and in considering the most effective combination treatment regimens.

Keywords

CPMAS; Mycobacteria; Cell walls; Antibiotics; Whole-cell NMR; Mycobacterium abscessus

*Corresponding author., cegelski@stanford.edu (L. Cegelski).

Declaration of Competing Interest

The authors declare that they have no known competing financial interests or personal relationships that could have appeared to influence the work reported in this paper.

Supplementary materials

Supplementary material associated with this article can be found, in the online version, at doi:10.1016/j.jmro.2023.100127.

Introduction

Since the discovery of penicillin by Alexander Fleming in 1928, modern antibiotics have saved millions of lives [1,2]. Today, however, we are still fighting against bacterial infections, and antibiotic resistance has become a major threat to public health globally [2]. In 2021, over 1.5 million people died from tuberculosis (TB), a disease caused by *Mycobacterium tuberculosis* (*Mtb*) [3]. Additionally, the incidence of non-tuberculous mycobacterial infection (NTM) has been increasing in the U.S. and globally [4–6]. Mycobacterial infections are highly prevalent among individuals suffering from chronic obstructive pulmonary disease (COPD) and individuals with suppressed immune systems. Individuals with COPD are the most at-risk for NTM lung disease and COPD is the 4th leading cause of death in the U.S. [7] NTM lung disease also afflicts cystic fibrosis (CF) patients, with most infected patients carrying a highly virulent strain of *Mycobacterium abscessus* [8]. Diseases caused by mycobacteria are difficult to treat and routinely involve combination treatment regimens to attempt to inhibit multiple targets required for mycobacterial survival [9,10]. The rise in *M. abscessus* infections is particularly alarming because of its resistance to classic anti-TB drugs as well as to most antibiotics that are currently available [11–13]. It is unclear why some anti-TB medications are not effective treatment options and differences in cell-wall composition may contribute to antibiotic treatment failures [14,15].

The mycobacterial cell wall is essential for cell growth and thus is an important target of antibiotics used to treat *Mtb* and NTM infections.[21] However, compared to Gram-positive and Gram-negative bacteria, mycobacteria assemble thicker and more complex cell walls, and exhibit reduced sensitivities to many cell-wall targeting agents used against these other bacteria. We lack a clear understanding of the reasons behind the failure of many cell-wall targeting antibiotics against mycobacteria [16]. This urges significant development to advance the introduction of new experimental approaches to define cell-wall composition in mycobacteria, to fully understand the modes of action of current antibiotics, and to introduce new strategies to treat *Mtb* and NTM infections [17–19].

The mycobacterial cell wall is assembled just outside the cell membrane with a general multilayered topology. The core layer nearest to the cell membrane is constructed of peptidoglycan (PG), the key component present also in Gram-positive and Gram-negative cell walls. Beyond PG, mycobacteria are unique in assembling arabinogalactan (AG), which is covalently attached to PG through a phosphoryl-N-acetylglucosaminosyl-rhamnosyl linkage [20–23] (Fig. 1A). This layer is followed by mycobacteria's hallmark waxy layer composed of mycolic acids (MA) and glycolipids. Collectively, the insoluble cell-wall complex containing these three components is referred to as the mycolyl-AG-PG complex, or mAGP. With more than 170 recognized species, the *Mycobacteriaceae* family shows great diversity in the types of diseases they cause and differences in antibiotic sensitivities [24]. Understanding the differences in chemical composition of cell walls will aid in effective and broad-spectrum therapeutic development.

Traditional methods to estimate mAGP composition and the relative abundance of the major components rely on hydrolysis and solubilization of mAGP, derivatization of PG and AG

fragments, and identification of liberated components by solution-based analyses. However, analyses based on these conventional approaches suffer from unavoidable incomplete solubilization and incomplete accounting of cell-wall parts [25,26]. The need to evaluate modes of action of mycobacterial cell-wall inhibitors more quantitatively has inspired our effort to develop a broadly applicable solid-state NMR platform in complex mycobacterial assemblies.

Solid-state NMR has a long history as a powerful analytical approach to define and characterize composition in complex organic and inorganic solids and materials. As relevant to work presented here, the CPMAS NMR examination of whole cells extends back 40 years ago to 1982 in early studies probing metabolism in soybean cotyledons [27]. Extensive work since then has also been directed to the study of bacteria, bacterial cell walls, and the bacterial extracellular matrix, motivated by the need for rigorous and quantitative parameters of composition and structure, particularly in non-crystalline and heterogeneous materials not amenable to solution-based analyses [28–32].

Herein, we report our efforts in developing an integrated approach leveraging bacteriology, biochemistry, and uniquely enabling solid-state NMR detection to provide an accounting of the major mycobacterial cell-wall components. These determinations complement extensive chemical and structural studies of detailed differences among individual cell-wall components, wherein chemical variations are found within the mycolic acids, and different types of linkages and peptidoglycan modifications are possible [33,34]. Our direct determinations capture the collective population of mycolic acids, PG, and AG, to determine the relative abundance of these mAGP components. The NMR spectra immediately reveal the completely distinct chemistry and carbon composition of each mAGP component and permitted a sum-of-the-parts reconstitution analysis to determine their relative abundance. We similarly employed this type of analysis to determine the relative abundance of PG and wall teichoic acids for *Staphylococcus aureus* cell walls *in situ* [35] and the relative abundance of extracellular matrix components produced by *Escherichia coli*, [36,37] *Vibrio cholerae*, [38] and the fungus *Aspergillus fumigatus* [39]. Moreover, our approach here with mycobacteria enables direct comparisons of mAGP composition among different species, different growth phases, and enables profiling of whole-cell changes resulting from antibiotic treatment. Specifically, *Mycobacterium smegmatis* was used as a model in our study, as most mycobacterial gene orthologs and cell-wall structures are conserved in this nonpathogenic species [40]. We extended our analysis to a human pathogen, *M. abscessus*, which immediately revealed that while the chemical components among different mycobacterial strains are preserved, their proportions can vary significantly.

Methods

Strains and growth conditions

M. smegmatis ATCC 700,084 and *M. abscessus* ATCC 19,977 were grown in Middlebrook 7H9 Broth with 0.2% glycerol, 10% ADC (albumin-dextrose-catalase) enrichment and 0.05% Tween-80. ADC enrichment was prepared according to the formula (8.5 g NaCl, 50 g BSA fraction V, 20 g dextrose, 0.03 g catalase per 1 L), filter sterilized and stored at 4 °C.

Whole-cell sample preparation

Each overnight cell culture was diluted 1:300 in 600 mL of media and grown at 37 °C with 200 rpm shaking to the desired optical density (OD) measured at 600 nm. Cells were centrifuged at 4 °C and 4400 g for 50 min to form a pellet. The pellet was washed 3 times with 5 mM HEPES buffer with centrifugation at 4 °C and 10,000 g for 10 min. The whole cells were frozen in liquid nitrogen and lyophilized.

mAGP isolation

Pure mAGP was isolated as described previously [41]. Briefly, whole cells were harvested as described above and frozen in liquid nitrogen. The whole-cell pellets (5 g wet weight) were left to thaw on ice, resuspended in 20 mL of breaking buffer (2% w/v Triton X-100 in PBS) and sonicated on ice for 10 cycles (60 s on, 90 s off). The crude cell wall was collected by centrifugation (30 min at 27,000 g, 4 °C), resuspended in 60 mL of breaking buffer and further extracted by stirring slowly overnight at room temperature (RT). Crude cell wall was collected by centrifugation (30 min at 27,000 g, 4 °C) and the pelleted cell-wall material was extracted three times with 100 mL of 2% SDS in PBS for 1 hour at 95 °C to remove nucleotides and associated proteins. SDS solution was removed between the boiling procedures by centrifugation (20 min at 27,000 g, RT). The pellet was washed successively with Milli-Q water two times, 80% acetone in water two times, and finally acetone (20 mL each) with centrifugation in between (30 min at 27,000 g, RT). The final pure mAGP complex was air-dried.

AGP isolation

Pure AGP was isolated from mAGP by treatment with base to release cell-wall bound mycolic acids, which were removed by extracting the pellet with organic solvent [42]. Isolated mAGP (60 mg) was transferred to Oak Ridge Teflon FEP tube, resuspended in 30 mL 0.5% KOH and stirred at 37 °C for 5 days. The pellet was recovered by centrifugation (30 min, 27,000 g, RT), washed with 30 mL of methanol, and collected by centrifugation as above. The pellet was resuspended in 24 mL of chloroform and stirred at RT for 30 min, followed by addition of 12 mL of methanol and centrifugation (30 min, 27,000 g at RT). The pellet was washed again with 30 mL methanol, collected by centrifugation as above and air-dried. The typical yield of AGP from mAGP was approximately 38% by dry mass.

PG isolation

PG was isolated as described previously with modifications [42]. Dry AGP complex was resuspended in 20 mL of 0.05 M sulfuric acid in a glass screw cap tube and slowly stirred at 37 °C for 4.5 days to remove AG. The pellet containing PG was obtained by centrifugation at 3000 g for 15 min. The pellet was washed three times with 10 mM Tris buffer (pH 8.2) with centrifugation after each rinse (30 min at 27,000 g, RT). The final pellet was resuspended in 5 mL MQ water, flash frozen in liquid nitrogen and lyophilized to obtain a pure white material *i.e.,* mycobacterial PG. The typical yield of PG from AGP was approximately 40% by dry mass.

Solid-state ^{13}C CPMAS NMR measurements

Solid-state ^{13}C CPMAS NMR [43] experiments were carried out in an 89-mm-bore 11.7T magnet using either an Agilent triple-resonance BioMAS probe with a DD2 console (Agilent Technologies) or a home-built four-frequency ^{1}H/^{19}F/^{13}C/^{15}N all-transmission-line probe with a Varian VNMRS console. Samples were spun at 7143 Hz in either 36-μl-capacity 3.2-mm zirconia rotors or thick-walled 5-mm-outer-diameter zirconia rotors. The field strength for cross-polarization was 50 kHz for ^{13}C with ramped CP at 57 kHz on ^{1}H for 1.5 ms. ^{1}H decoupling was performed at 83 kHz. The recycle time was 2 s for all experiments. Spectrometer ^{13}C chemical shift referencing was performed by setting the high-frequency adamantane peak to 38.5 ppm [44]. All spectra, except those obtained for the CP array experiments (Fig. S3 and S4), were the result of 40,960 scans. CP array experiments were performed at 0.25, 0.5, 1, 1.5, 2, 3, 4, 5, 6 ms. 8192 scans were collected for the CP array experiment of *M. smegmatis* mAGP. 16,384 scans were collected for the CP array experiment of *M. abscessus* mAGP.

Results and discussion

Spectral assignment of M. smegmatis mAGP complex components from natural abundance ^{13}C CPMAS NMR

The first step in cell-wall analysis for mycobacteria involves isolation of mAGP. In biochemical studies, this is usually followed by extensive chemical and enzymatic digestions to separate components and partially solubilize components into low molecular weight species for analysis, typically by liquid chromatography mass spectrometry [25]. The still insoluble high molecular weight material that remains is not accounted for in these conventional approaches. We envisioned being able to isolate mAGP and directly compare the ^{13}C CPMAS NMR spectrum of mAGP with spectra of isolated constituent parts, namely PG, AG, and MA, to report on cell-wall composition and to provide a powerful approach for the direct comparison of different mAGP complexes.

^{13}C CPMAS spectra of isolated mAGP from *M. smegmatis* harvested at different cell densities were nearly identical (Fig. 1B), indicating that the ratios of PG, AG, and MA are constant for *M. smegmatis* during these time points in the exponential growth phase. Further analysis was performed using mAGP isolated from cells harvested at the OD_{600} of 3.0. Individual carbon types in the mAGP CPMAS spectrum could be assigned according to the chemical shifts consistent with the chemical structure of each component, as annotated in Fig. 1C. Furthermore, for additional power in direct spectroscopic comparisons, we removed the MA through alkaline hydrolysis to leave behind the insoluble AGP [42]. As anticipated, this AGP sample spectrum lacks the salient MA methylene intensity near 30 ppm and the sharp lipid alkene contributions at 130 ppm that are features of unsaturated MA in *M. smegmatis* and observed in the full mAGP spectrum (Fig. 1C).

To further analyze the AGP spectrum, we isolated PG which can be obtained in good yield. PG is the only mAGP component containing amino acids. The PG spectrum contains chemical shifts consistent with amino acid intensities (carbonyl and Cα carbons) and the N-acetylglucosamine and N-acetylmuramic acid sugar backbone intensities (Fig. 1D) [20].

The difference in intensity between the AGP and the PG spectrum is consistent with our expectations of isolated AG. The required acid hydrolysis to release AG from AGP complexes resulted in too low a yield of AG to directly evaluate by CPMAS. Thus, to further explore the spectra, a theoretical spectrum of AG was obtained by subtracting the PG spectrum from the AGP spectrum. We compared this spectral subtraction with a CPMAS spectrum of the only type of commercially available AG sample, which is obtained from a plant. In this case, we obtained an experimental CPMAS spectrum of the commonly studied Larchwood AG (Fig. S1). The AGP-PG difference spectrum and the Larchwood AG spectrum contained two similar broad peaks, one associated with anomeric carbons (100 to 110 ppm) and the other with major polysaccharide carbons in AG (60 to 80 ppm). There is a general difference in the span of these two regions between each sample due to the differences in sugars present in plant and microbial arabinogalactan and possible variation in intermolecular packing patterns between mycobacteria and Larchwood AG [21,45]. Similar differences have been characterized in highly studied cellulose samples from plants and various microorganisms [46]. Overall, through comparison of the *M. smegmatis* mAGP, AGP, and PG spectra, we were able to identify each component in the mAGP spectrum (Fig. 1C).

Characterization of cross polarization for mAGP and PG complexes

The CPMAS NMR spectra in Fig. 1 highlight the power in using natural abundance ^{13}C CPMAS to examine cell walls and mAGP components in mycobacteria, adding to numerous examples in other complex and heterogeneous biological solids since the introduction of CPMAS NMR almost 50 years ago [43]. Towards our next goal of using CPMAS NMR spectra to estimate the relative abundance of mAGP components in mAGP samples, we characterized the cross polarization behavior of carbons in the mAGP spectrum through quantitative CP array analysis. In particular, one wants to evaluate whether distinct carbons within a sample or certain carbons in the context of different samples exhibit comparable CP behavior or might differ dramatically in the extents of CP efficiency from ^{1}H nuclei to ^{13}C nuclei, *i.e.* the buildup of magnetization, and/or in the relaxation dictated by $T_{1\rho}(H)$, the proton spin–lattice relaxation time in the rotating frame [47,48]. For well behaved biological solids, the CP array experiment is also often used to determine absolute peak intensities or peak areas of individual chemically shift resolved carbon contributions within a single spectrum [48]. The multiCP pulse sequence has also been used for this purpose [49].

Spectra of *M. smegmatis* mAGP obtained with different CP times exhibited a typical increase and slow decrease in signal intensity for carbons across the spectrum (Fig. 1E), similar to our published results with comparable types of lyophilized biological solids, including mixed peptide-glycan composites present in bacterial cell walls, extracellular matrix materials, and butterfly chrysalides [35,39,50]. Peak intensities for shift-resolved carbons revealed comparable slopes of decay, revealing similar $T_{1\rho}(H)$ relaxation for mAGP carbons (Fig. 1F).

Bottom-up reconstitution and estimation of PG, AG, and ma contributions to the M. smegmatis mAGP complex

We performed a reconstitution analysis using a bottom-up "sum-of-the-parts" approach [29,35,36] for the *M. smegmatis* mAGP. We sought a semi-quantitative estimation of each component in the actual *in situ* mAGP complex without digestions and loss of constituents as is inevitable for biochemical analysis. For the individual "parts," we obtained ^{13}C CPMAS spectra of the PG we isolated from *M. smegmatis*, commercially available AG from Larchwood, and commercially available MA from *M. tuberculosis* (Fig. 2A). The *M. tuberculosis* MA spectrum lacks the unsaturation (alkenes) present in the *M. smegmatis* mAGP spectrum due to differences in MA composition [51]. As also noted above, the Larchwood AG chemical shifts are slightly shifted from those we attributed to AG in the mAGP spectrum. We normalized each component spectrum according to its mass and accounted for the scaling necessary to obtain a spectral sum that closely recapitulated the CPMAS spectrum of the *M. smegmatis* mAGP introduced above (Fig. 2B). A reasonable fit of the spectral sum to the nearest increment of 5% was obtained with mass scaling of ^{13}C spectra as: 50% PG, 20% AG, and 30% MA (Fig. 2B). Notably, the reconstitution shows comparable intensities for the major PG-associated peaks, *i.e.*, the carbonyls centered at 175 ppm, the Cα contributions (50–60 ppm), and AG carbons (near to 80 ppm, noting the shift between Larchwood and mycobacteria). It is challenging to determine a definitive error margin for this percent carbon intensity analysis. However, we compare the result with two additional reconstitutions to show the clear differences in the scaled sums and poor fit of other ratios to the mAGP complex. The scaled sum using equal contributions of 33.3% PG, 33.3% AG, and 33.3% MA (Fig. S2A) does not yield enough intensity in the PG carbonyl (175 ppm) and Cα regions (50–60 ppm). In another example, the scaled sum of 40% PG, 40% AG, and 20% MA (Fig. S2B) also did not produce enough signal intensity for the PG carbons or for the aliphatic carbons in MA (30 ppm). Thus, PG must be present in greater abundance in mAGP and our most reasonable fit was obtained with 50% PG, 20% AG, and 30% MA (Fig. 2B).

Comparison of mAGP from M. abscessus and from M. smegmatis

We directly compared the ^{13}C CPMAS spectra of isolated mAGP from two mycobacterial species, *M. abscessus*, which is the most difficult NTM infection to treat especially in COPD, and *M. smegmatis*. There was a detectable decrease in the contributions of MA and a more significant decrease in that of PG in mAGP isolated from *M. abscessus* compared to *M. smegmatis* (Fig. 3A). Quantitative CP array analysis revealed comparable CP behavior of carbons in the *M. abscessus* mAGP as in the *M. smegmatis* mAGP (Fig. 1F and S3); of selected key carbons (carbonyls) in PG isolated from *M. smegmatis* as compared to the mAGP sample; and of methylene carbons in MA isolated from *M. tuberculosis* as compared to the mAGP sample (Fig. S4). Using the reconstitution analysis of cell-wall parts, we show that the ^{13}C CPMAS mAGP spectrum of *M. abscessus* is achieved with mass percentages of 35% PG, 35% AG, and 30% MA, rounded to the nearest 5% (Fig. 3B). The variations in AG and PG levels between *M. abscessus* and *M. smegmatis* may underlie different antibiotic sensitivities when other commonly attributed biochemical differences do not appear to be responsible. Future work will be directed to building more comparisons between different strains, growth conditions, and antibiotic treatments.

Antibiotic modes of action through whole-cell NMR

We previously demonstrated great power in evaluating the modes of action of antibiotics against the Gram-positive pathogen *S. aureus* through whole-cell NMR to evaluate the direct compositional changes in carbon pools observed in antibiotic-treated cells [52]. For example, cell-wall inhibitors such as vancomycin resulted in reduced cell-wall content and revealed reductions in nucleotide pools due to catabolism attributed to metabolic stress and routing to PG precursors [30,35,52, 53]. This approach had also revealed unanticipated compensation of cells under the stress of cell-wall inhibitor treatment. Specifically, tunicamycin is known to inhibit the biosynthesis of teichoic acid. We observed reduced teichoic acid content, but also increased peptidoglycan content, potentially as cells attempted to compensate for reduced cell-wall integrity from loss of teichoic acid [35]. Here, we sought to determine whether whole-cell NMR of mycobacteria would similarly be sensitive to revealing the influence of antibiotics. We employed vancomycin, which also kills mycobacteria, and isoniazid, which is a common antibiotic used in mycobacterial infection treatment regimens.

Vancomycin exerts its influence through binding uncrosslinked D-Ala-D-Ala-termini of immature PG and Lipid II PG precursors still associated with the cell membrane. This activity sequesters Lipid II and prevents incorporation of PG precursors, vis-à-vis transglycosylation, into growing PG strands [54]. The ^{13}C CPMAS spectrum of vancomycin-treated *M. smegmatis* whole cells revealed a significant decrease in cell-wall contributions, similar to that observed for *S. aureus* [52]. In *M. smegmatis*, we see reductions attributed to PG and AG (which would be attached to PG) (Fig. 4A). We also investigated the influence of isoniazid treatment. Isoniazid inhibits mycolic acid synthesis [55]. As anticipated, we observed signal diminution for aliphatic carbons in MA compared to the untreated control (Fig. 4B). In addition, we observed an increase in intensity at 70 ppm, consistent with an accumulation of trehalose, a documented effect of isoniazid on mycobacteria [56]. In summary, these spectral benchmarks provide non-invasive spectral reporting of carbon composition to shed light on the whole-cell influence of antibiotics.

Conclusions and future perspectives

Clinical treatment of TB and NTM infections requires prolonged combination drug therapy. Monotherapy cannot be employed to treat disease because of the high probability of inducing drug resistance. Consequently, it is essential that several drugs be administered concurrently to maximize sterilizing conditions. Historically, this has been achieved by administering multiple drugs orally. However, with limited options for improved treatment, and an absence of a robust pipeline of new drugs, new strategies are urgently needed in new drug discovery and in optimizing dosage and combinations of currently available therapeutics. The urgency of this grand challenge motivates the deployment of new analytical approaches to measure and quantify composition of mycobacterial cell walls and evaluate how composition actually changes through combination treatments for different lengths of time. This could contribute new knowledge for considering and identifying preferred antibiotic combinations. The cell wall provides mycobacteria a formidable

protective barrier, but also presents a tremendous therapeutic opportunity as the Achilles heel of mycobacterial survival and persistence in the host.

We have introduced an approach to directly measure mycobacterial cell-wall composition through non-invasive natural abundance ^{13}C CPMAS detection of mAGP. We report on the first quantitative determination of the composition of *M. smegmatis* and *M. abscessus* cell-wall envelope using a bottom-up reconstitution approach. Our NMR analysis allowed us to understand the composition of the mycobacterial cell-wall complex at the individual component level and extend this knowledge to intact whole cells, which is otherwise challenging to analyze. Importantly, mAGP spectra of *M. abscessus* revealed significantly more AG and less PG in mAGP as compared to *M. smegmatis. M. abscessus* is the most difficult NTM infection to treat, especially in COPD, and this definitive conclusion on cell-wall composition will guide new experiments to test hypotheses regarding possible correlations of the AG-to-PG ratio and antibiotic susceptibilities. Future work will examine additional strains and species of the *Mycobacteriaceae* family to fully map compositional profiles and connect these with antibiotic susceptibilities. We also revealed that solid-state NMR has the potential to allow direct comparisons of the effects of antibiotics, providing holistic atomic-level compositional insight accompanying antibiotic activity in whole cells. In conclusion, our results position solid-state NMR as a powerful tool to detect and define cell-wall composition of mycobacteria and to evaluate the molecular influence of antibiotics by cell-wall and whole-cell NMR.

Supplementary Material

Refer to Web version on PubMed Central for supplementary material.

Acknowledgements

This research was supported in part by the National Institutes of Health grant R01GM117278 (L.C.) and in part by a Cystic Fibrosis Foundation Postdoctoral Fellowship (J.B.). This work was also supported by the Department of Defense, through the DoD Peer Reviewed Medical Research Program Technology/Therapeutic Development Program under Award No. W81XWH1810765 (to G.C.). Opinions, interpretations, conclusions and recommendations are those of the authors and are not necessarily endorsed by the Department of Defense.

Data availability

Data will be made available on request.

References

[1]. Fleming A, Classics in infectious diseases: on the antibacterial action of cultures of a penicillium, with special reference to their use in the isolation of B. influenzae, Br. J. Exp. Pathol 10 (1929) 226–236.

[2]. Piddock LJV, The crisis of no new antibiotics—what is the way forward? Lancet Infect. Dis 12 (2012) 249–253. [PubMed: 22101066]

[3]. Wolrd Health Organization, Global tuberculosis report 2022, n.d.

[4]. Fifor A, Krukowski K, Honda JR, Sex, ancestry, senescence, and aging (SAnSA) are stark drivers of nontuberculous mycobacterial pulmonary disease, J. Clin. Tuberc. Other. Mycobact. Dis 26 (2022), 100297. [PubMed: 35059508]

[5]. Prevots DR, Marras TK, Epidemiology of human pulmonary infection with nontuberculous mycobacteria: a review, Clin. Chest. Med 36 (2015) 13–34, 10.1016/j.ccm.2014.10.002. [PubMed: 25676516]

[6]. Donohue MJ, Increasing nontuberculous mycobacteria reporting rates and species diversity identified in clinical laboratory reports, BMC Infect. Dis 18 (2018) 163, 10.1186/s12879-018-3043-7. [PubMed: 29631541]

[7]. Soriano, Prevalence and attributable health burden of chronic respiratory diseases, 1990–2017: a systematic analysis for the Global Burden of Disease Study 2017, Lancet Respir. Med 8 (2020) 585–596, 10.1016/S2213-2600(20)30105-3. [PubMed: 32526187]

[8]. Bryant, Emergence and spread of a human-transmissible multidrug-resistant nontuberculous mycobacterium, Science (80-.) 354 (2016) 751–757.

[9]. Gygli SM, Borrell S, Trauner A, Gagneux S, Antimicrobial resistance in Mycobacterium tuberculosis: mechanistic and evolutionary perspectives, FEMS Microbiol. Rev 41 (2017) 354–373, 10.1093/femsre/fux011. [PubMed: 28369307]

[10]. Gopalaswamy R, Shanmugam S, et al. , Mondal, Of tuberculosis and non-tuberculous mycobacterial infections – a comparative analysis of epidemiology, diagnosis and treatment, J. Biomed. Sci 27 (2020) 74, 10.1186/s12929-020-00667-6. [PubMed: 32552732]

[11]. Nessar R, Cambau E, Reyrat JM, Murray A, Gicquel B, Mycobacterium abscessus: a new antibiotic nightmare, J.. Antimicrob Chemother 67 (2012) 810–818. [PubMed: 22290346]

[12]. Lopeman RC, Harrison J, Desai M, Cox JAG, Mycobacterium abscessus: environmental bacterium turned clinical nightmare, Microorganisms 7 (2019) 90. [PubMed: 30909391]

[13]. Johansen MD, Herrmann JL, Kremer L, Non-tuberculous mycobacteria and the rise of Mycobacterium abscessus, Nat. Rev. Microbiol 18 (2020) 392–407. [PubMed: 32086501]

[14]. Brode SK, Daley CL, Marras TK, The epidemiologic relationship between tuberculosis and non-tuberculous mycobacterial disease: a systematic review, Int. J. Tuberc. Lung. Dis 18 (2014) 1370–1377. [PubMed: 25299873]

[15]. Soni I, De Groote MA, Dasgupta A, Chopra S, Challenges facing the drug discovery pipeline for non-tuberculous mycobacteria, J. Med. Microbiol 65 (2016) 1–8. [PubMed: 26515915]

[16]. Abdelaal HFM, Chan ED, Young L, Baldwin SL, Coler RN, Mycobacterium abscessus: it's Complex, Microorganisms 10 (2022) 1454. 10.3390/microorganisms10071454. [PubMed: 35889173]

[17]. Goossens SN, Sampson SL, Van Rie A, Mechanisms of Drug-Induced Tolerance in Mycobacterium tuberculosis, Clin. Microbiol. Rev 34 (2020) e00141–20. [PubMed: 33055230]

[18]. Batt SM, Burke CE, Moorey AR, Besra GS, Antibiotics and resistance: the two-sided coin of the mycobacterial cell wall, Cell Surf 6 (2020), 100044, 10.1016/j.tcsw.2020.100044. [PubMed: 32995684]

[19]. Jarlier V, Nikaido H, Mycobacterial cell wall: structure and role in natural resistance to antibiotics, FEMS Microbiol. Lett 123 (1994) 11–18, 10.1111/j.1574-6968.1994.tb07194.x. [PubMed: 7988876]

[20]. Abrahams KA, Besra GS, Mycobacterial cell wall biosynthesis: a multifaceted antibiotic target, Parasitology 145 (2018) 116–133. [PubMed: 27976597]

[21]. Brennan PJ, Spencer JS, The physiology of Mycobacterium leprae, in: Scollard DM, Gilligs TP (Eds.), Int. Textb. Lepr, 2019.

[22]. McNeil M, Daffe M, Brennan PJ, Evidence for the nature of the link between the arabinogalactan and peptidoglycan of mycobacterial cell walls, J. Biol. Chem 265 (1990) 18200–18206. [PubMed: 2211696]

[23]. Maitra A, Munshi T, Healy J, Martin LT, Vollmer W, Keep NH, Bhakta S, Cell wall peptidoglycan in Mycobacterium tuberculosis: an Achilles' heel for the TB-causing pathogen, FEMS Microbiol. Rev 43 (2019) 548–575. [PubMed: 31183501]

[24]. Forbes BA, Mycobacterial taxonomy, J. Clin. Microbiol 55 (2017) 380–383. [PubMed: 27927928]

[25]. Bhamidi S, Shi L, Chatterjee D, Belisle JT, Crick DC, McNeil MR, A bioanalytical method to determine the cell wall composition of Mycobacterium tuberculosis grown in vivo, Anal. Biochem 421 (2012) 240–249. [PubMed: 22107887]

[26]. Bhamidi S, Scherman MS, Jones V, Crick DC, Belisle JT, Brennan PJ, McNeil MR, Detailed structural and quantitative analysis reveals the spatial organization of the cell walls of in vivo grown Mycobacterium leprae and in vitro grown Mycobacterium tuberculosis, J. Biol. Chem 286 (2011) 23168–23177. [PubMed: 21555513]

[27]. Skokut TA, Varner JE, Schaefer J, Stejskal EO, McKay RA, N- and [C]NMR determination of utilization of glycine for synthesis of storage protein in the presence of glutamine in developing cotyledons of soybean, Plant Physiol 69 (1982) 314–316. [PubMed: 16662199]

[28]. Reichhardt C, Cegelski L, Solid-state NMR for bacterial biofilms, Mol. Phys 112 (2014) 887–894. [PubMed: 24976646]

[29]. Cegelski L, Bottom-up and top-down solid-state NMR approaches for bacterial biofilm matrix composition, J. Magn. Reson 253 (2015) 91–97. [PubMed: 25797008]

[30]. Romaniuk JAH, Cegelski L, Bacterial cell wall composition and the influence of antibiotics by cell-wall and whole-cell NMR, Phil. Trans. R. Soc. B 370 (2015), 20150024. [PubMed: 26370936]

[31]. Reichhardt C, Joubert L, Clemons KV, Stevens DA, Cegelski L, Integration of electron microscopy and solid-state NMR analysis for new views and compositional parameters of Aspergillus fumigatus biofilms, Med. Mycol 57 (2019) S239–S244. [PubMed: 30816969]

[32]. Ghassemi N, Poulhazan A, Deligey F, Mentink-Vigier F, Marcotte I, Wang T, Solid-state NMR investigations of extracellular matrixes and cell walls of Algae, Bacteria, Fungi, and plants, Chem. Rev 122 (2022) 10036–10086. [PubMed: 34878762]

[33]. Barry CE 3rd, Lee RE, Mdluli K, Sampson AE, Schroeder BG, Slayden RA, Yuan Y, Mycolic acids: structure, biosynthesis and physiological functions, Prog. Lipid. Res 37 (1998) 143–179. [PubMed: 9829124]

[34]. Vollmer W, Blanot D, M… de Pedro, Peptidoglycan structure and architecture, FEMS Microbiol. Rev 32 (2008) 149–167. [PubMed: 18194336]

[35]. Romaniuk JAH, Cegelski L, Peptidoglycan and Teichoic acid levels and Alterations in Staphylococcus aureus by Cell-Wall and Whole-Cell Nuclear Magnetic Resonance, Biochemistry 57 (2018) 3966–3975, 10.1021/acs.biochem.8b00495. [PubMed: 29806458]

[36]. McCrate OA, Zhou X, Reichhardt C, Cegelski L, Sum of the Parts: composition and Architecture of the Bacterial Extracellular Matrix, J. Mol. Biol 425 (2013) 4286–4294, 10.1016/j.jmb.2013.06.022. [PubMed: 23827139]

[37]. Jeffries J, Thongsomboon W, Visser JA, Enriquez K, Yager D, Cegelski L, Variation in the ratio of curli and phosphoethanolamine cellulose associated with biofilm architecture and properties, Biopolymers 112 (2021) e23395. [PubMed: 32894594]

[38]. Reichhardt C, Fong JC, Yildiz F, Cegelski L, Characterization of the Vibrio cholerae extracellular matrix: a top-down solid-state NMR approach, Biochim. Biophys. Acta 1848 (2015) 378–383. [PubMed: 24911407]

[39]. Reichhardt C, Ferreira JA, Joubert LM, Clemons KV, Stevens DA, Cegelski L, Analysis of the Aspergillus fumigatus Biofilm Extracellular Matrix by Solid-State Nuclear Magnetic Resonance Spectroscopy, Eukaryot. Cell 14 (2015) 1064–1072. [PubMed: 26163318]

[40]. Sparks IL, Derbyshire KM, Jacobs WRJ, Morita YS, Mycobacterium smegmatis: the Vanguard of Mycobacterial Research, J. Bacteriol 205 (2023), e0033722, 10.1128/jb.00337-22. [PubMed: 36598232]

[41]. Besra GS, Preparation of Cell-Wall Fractions from Mycobacteria, in: Parish T, Stoker NG (Eds.), Mycobact. Protoc. Methods Mol. Biol Vol 101, Humana Press, 1998, pp. 91–107, 10.1385/0-89603-471-2:91.

[42]. Grzegorzewicz AE, Jackson M, Subfractionation and Analysis of the Cell Envelope (Lipo)polysaccharides of Mycobacterium tuberculosis, in: Delcour A (Ed.), Bact. Cell Surfaces. Methods Mol. Biol Vol 966, Humana Press, 2013, pp. 309–324, 10.1007/978-1-62703-245-2_19.

[43]. Schaefer J, Stejskal EO, Carbon-13 nuclear magnetic resonance of polymers spinning at the magic angle, J. Am. Chem. Soc 98 (1976) 1031–1032.

[44]. Morcombe CR, Zilm KW, Chemical shift referencing in MAS solid state NMR, J. Magn. Reson 162 (2003) 479–486. [PubMed: 12810033]

[45]. López-Franco YL, Higuera-Ciapara I, Lizardi-Mendoza J…, Wang W, Goycoolea FM, Chapter 23 - Other exudates: tragacanth, karaya, mesquite gum, and larchwood arabinogalactan, in: Phillips GO, Williams PA (Eds.), Woodhead Publ. Ser. Food Sci. Technol. Nutr. Handb. Hydrocoll, 3rd Ed, Woodhead, 2021, pp. 673–727, 10.1016/B978-0-12-820104-6.00003-6. .

[46]. Wang T, Yang H, Kubicki JD, Hong M, Cellulose structural polymorphism in plant primary cell walls investigated by High-Field 2D solid-state NMR Spectroscopy and Density Functional Theory Calculations, Biomacromolecules 17 (2016) 2210–2222, 10.1021/acs.biomac.6b00441. [PubMed: 27192562]

[47]. Stejskal E…, Schaefer J, Steger TR, High-resolution 13C nuclear magnetic resonance in solids, Faraday Symp. Chem. Soc 13 (1978) 56–62.

[48]. Kolodziejski W, Klinowski J, Kinetics of cross-polarization in solid-state NMR: a guide for chemists, Chem. Rev 102 (2002) 613–628. [PubMed: 11890752]

[49]. Johnson RL, Schmidt-Rohr K, Quantitative solid-state 13C NMR with signal enhancement by multiple cross polarization, J. Magn. Reson 239 (2014) 44–49. [PubMed: 24374751]

[50]. Goularte NF, Kallem T, Cegelski L, Chemical and molecular composition of the chrysalis reveals common chitin-rich structural framework for monarchs and swallowtails, J. Mol. Biol 434 (2022), 167456. [PubMed: 35045329]

[51]. Marrakchi H, Lanelle MA, Daffe M, Mycolic acids: structures, biosynthesis, and beyond, Chem. Biol 21 (2014) 67–85, 10.1016/j.chembiol.2013.11.011. [PubMed: 24374164]

[52]. Nygaard R, Romaniuk JAH, Rice DM, Cegelski L, Spectral snapshots of bacterial cell-wall composition and the influence of antibiotics by whole-cell NMR, Biophys. J 108 (2015) 1380–1389, 10.1016/j.bpj.2015.01.037. [PubMed: 25809251]

[53]. Cegelski L, Hing AW, Kim SJ, Studelska DR, O'Connor RD, Mehta AK, Schaefer J, REDOR characterization of Vancomycin mode of action in S. aureus, Biochemistry 41 (2002) 13053–13058. [PubMed: 12390033]

[54]. Reynolds PE, Structure, biochemistry and mechanism of action of glycopeptide antibiotics, Eur. J. Clin. Microbiol. Infect. Dis 8 (1989) 943–950. [PubMed: 2532132]

[55]. Takayama K, Davidson LA, Antimycobacterial drugs that inhibit mycolic acid synthesis, Trends. Biochem. Sci 4 (1979) 280–282, 10.1016/0968-0004(79)90301-3.

[56]. Winder FG, Brennan PJ, McDonnell I, Effects of isoniazid on the composition of mycobacteria, with particular reference to soluble carbohydrates and related substances, Biochem. J 104 (1967) 385–393, 10.1042/bj1040385. [PubMed: 6048780]

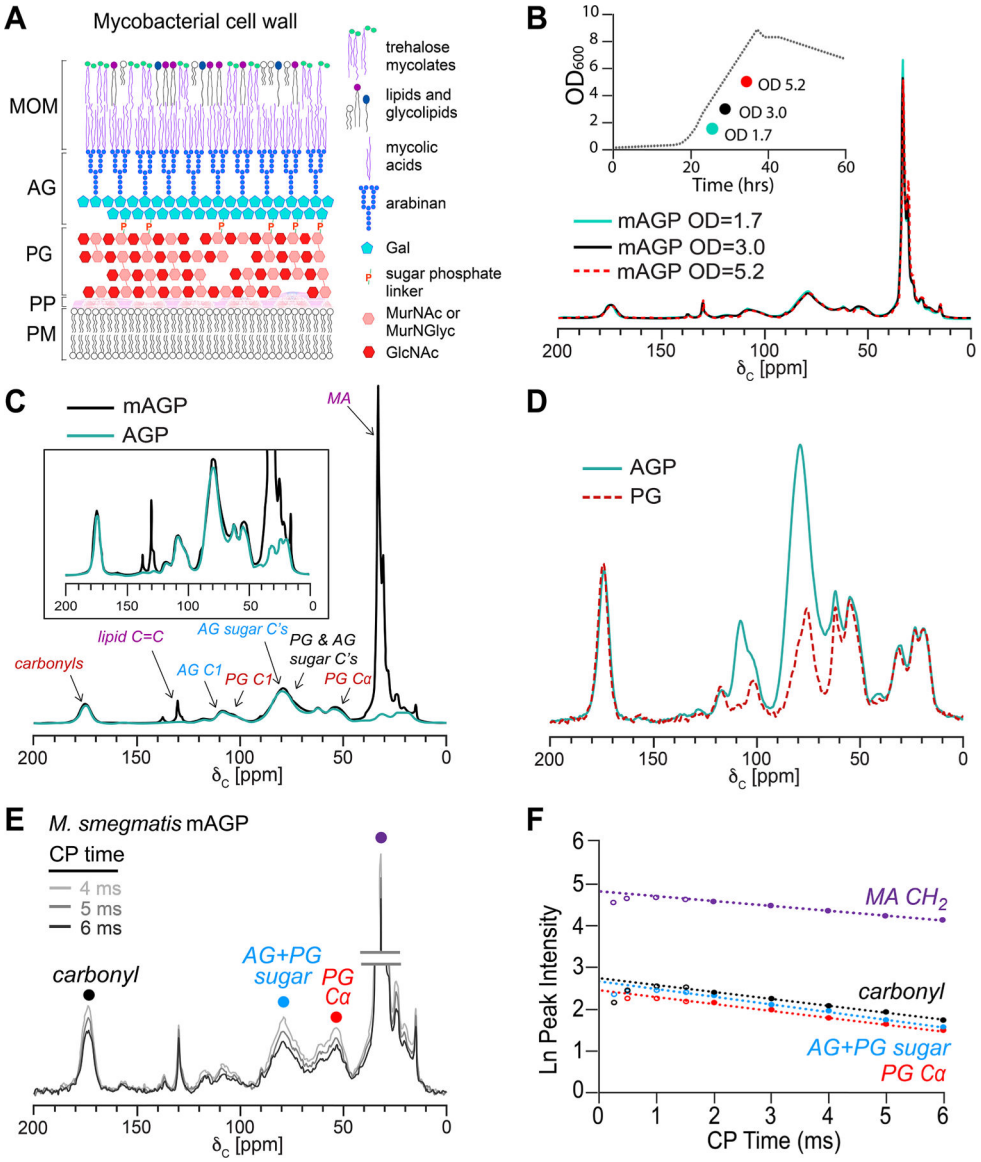

Fig. 1.

(A) Mycobacterial cell-wall compositions. (B) ^{13}C CPMAS spectra of mAGP from *M. smegmatis* at OD 1.7, OD 3.0, and OD 5.2. Inset shows the growth curve of *M. smegmatis* in Middlebrook 7H9 Broth with 0.2% glycerol, 10% ADC enrichment and 0.05% Tween-80. (C) ^{13}C CPMAS spectra comparison of *M. smegmatis* mAGP from cells harvested at OD 3.0, and the isolated AGP after removal of MA. (D) ^{13}C CPMAS spectral comparison of *M. smegmatis* AGP and PG isolated from cells harvested at OD 3.0. Each spectrum is the result of 40,960 scans with sample masses of 22.3 mg mAGP and 7.7 mg PG. (E) ^{13}C CPMAS spectral comparison of *M. smegmatis* mAGP harvested at OD 1.0 with spectra acquired as a function of CP time (10.7 mg, 8192 scans each spectrum). (F) Quantitative CP array plot of selected peak intensities of *M. smegmatis* mAGP spectra obtained as a function of CP time.

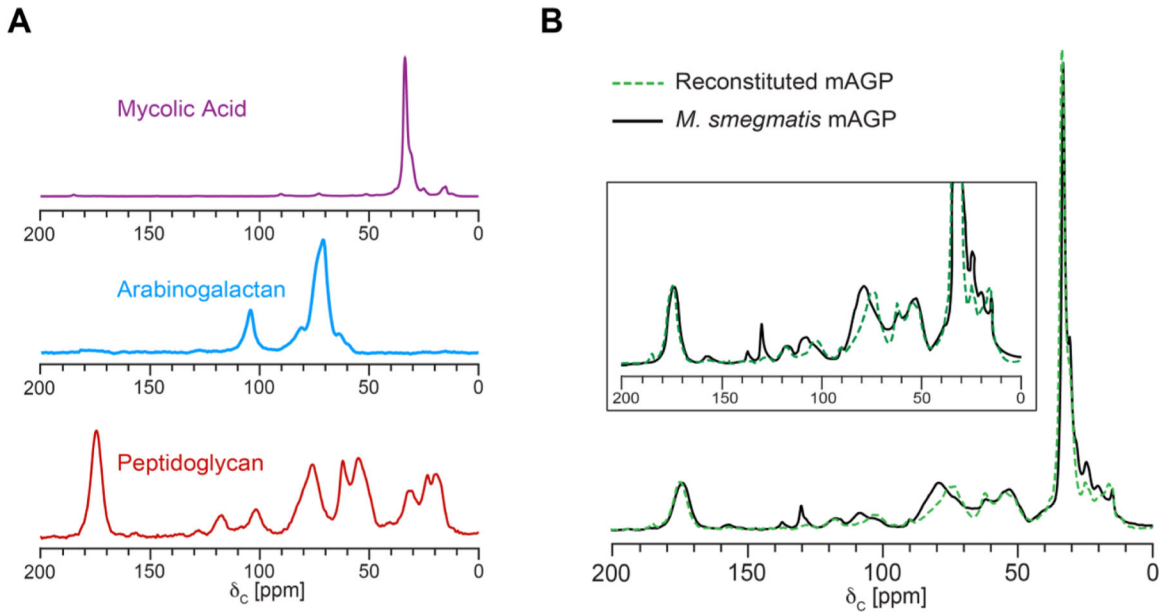

Fig. 2.

(A) ^{13}C CPMAS spectra of pure MA from *M. tuberculosis* (15.3 mg), AG from Larchwood (28.2 mg), and PG isolated from *M. smegmatis* (7.7 mg). (B) ^{13}C CPMAS spectrum of *M. smegmatis* mAGP from cells harvested at OD 1.0, and a reconstituted spectrum generated by adding 50% PG, 20% AG, and 30% AG from spectra in Fig. 2A. Each spectrum is the result of 40,960 scans.

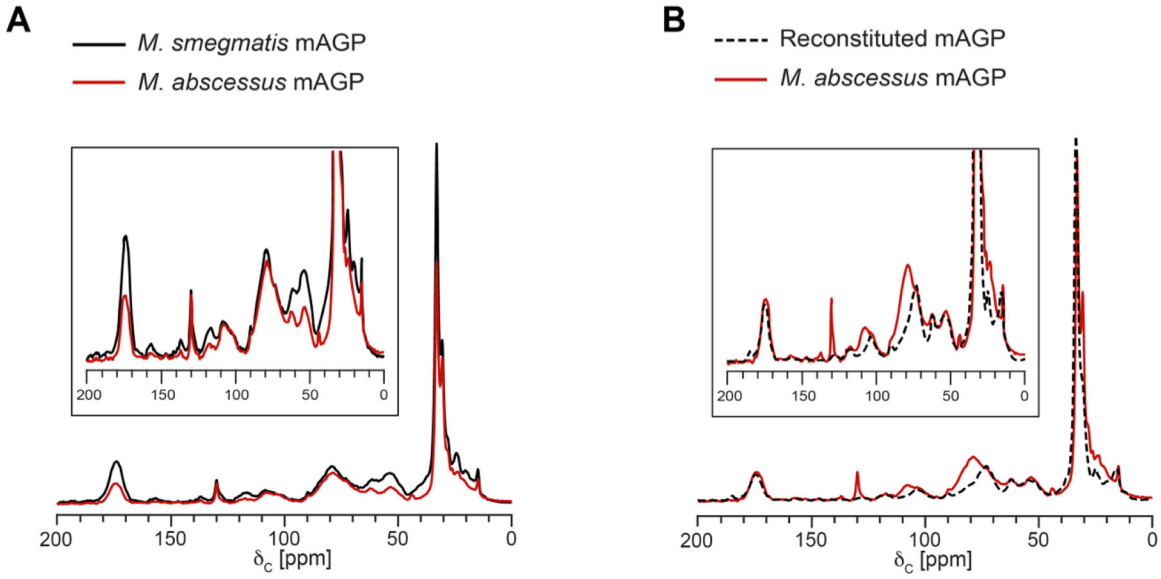

Fig. 3.

(A) ^{13}C CPMAS spectra of mAGP from *M. smegmatis* at OD 1.0 (24.5 mg), and mAGP from *M. abscessus* at OD 0.92 (10.3 mg). (B) ^{13}C CPMAS spectral overlay of the *M. abscessus* mAGP and a reconstituted spectrum generated by adding 35% PG, 35% AG, and 30% MA from spectra in Fig. 2A. Each spectrum is the result of 40,960 scans.

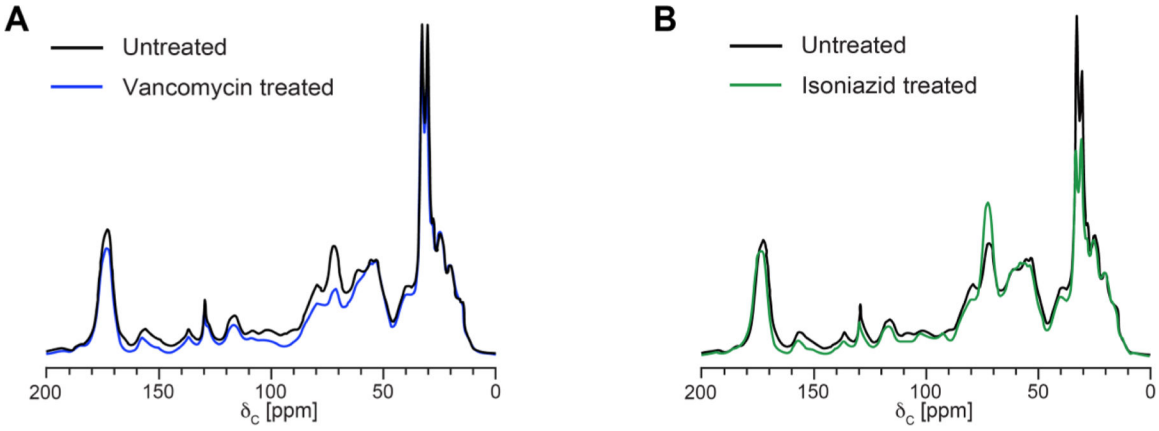

Fig. 4.

(A) CPMAS spectra of untreated *M. smegmatis* whole cells (OD 0.41, 31.3 mg) and vancomycin (80 μM, 10xMIC) treated *M. smegmatis* whole cells after 8 h (treated at OD 0.58, harvested at OD 0.53, 50 mg). (B) CPMAS spectra of untreated *M. smegmatis* (OD 0.94, 57.9 mg) and isoniazid-treated (80 μg/mL, 10xMIC) whole cells after 8 h (treated at OD 0.54, harvested at OD 1.6, 46 mg). Each spectrum is the result of 40,960 scans.